X-RAYS OF STELLAR CORONAE WITH CHANDRA AND XMM-NEWTON: DENSITIES AND STRUCTURES IN STELLAR CORONAE

J.-U. Ness

Hamburger Sternwarte, Gojenbergsweg 112, 21029 Hamburg, Germany

Abstract

The investigation of the coronal properties of magnetically active stars is presently being pushed forward by high-resolution X-ray spectroscopy. The measurement of electron densities can only be carried out by measurement of individual emission lines produced or suppressed by collisions between excited levels. The X-ray gratings on board XMM-Newton and Chandra provide sufficient spectral resolution and sensitivity to measure such lines. Prior to these missions density sensitive lines in the UV range measured with, e.g., EUVE, have been used to constrain electron densities. Some of these measurements can be repeated with Chandra LETGS, but earlier reports of densities as high as $10^{13}\,\mathrm{cm}^{-3}$ must be ruled out from the Chandra measurements. At present there is no evidence of consistently high densities in hot coronal plasma, neither from Fe XXI lines nor from high-Z He-like triplets. The low-Z He-like triplets (O VII and Ne IX) probe different regions of the temperature distribution. In a large survey of density measurements the 'hotter' Ne IX ions result in systematically higher densities than the O VII diagnostics implying different pressures and thus distinct emission regions. The density measurements allow estimates of the emitting volumes and the extent of the stellar coronae above the stellar surface. Application of the most standard basic scaling law by Rosner et al. (1978) results in a trend of volume filling factors which increase with activity for the higher-pressure regions probed with Ne IX, but not for the cooler plasma probed by O VII.

Key words: Stars: structure – X-ray: spectroscopy – Stars: coronae

1. Introduction

The extreme physical properties of the solar corona have been a surprise, when piece by piece high temperatures and low densities have been discovered. Measurements of the optical corona revealed that the spectrum is almost identical to the spectrum of the solar photosphere at all heights, suggesting scattering of photospheric light by electrons. Since most Fraunhofer lines could not be identified and the strongest lines were found smeared out, Grotrian (1931) concluded that the electrons must have extremely high mean velocities of $7.5 \times 10^8\,\mathrm{cm\,s}^{-1}$ leading to Doppler broadening. This finding could have already led to the conclusion of temperatures in the range of several hundred thousand up to a million degrees, but only the identification of emission lines from highly ionized species led to the undoubted conclusion of the million degree corona (e.g., Edlén 1943; Grotrian 1939). This high temperature requires X-ray observations in order to directly look into the million degree plasma. Past X-ray missions like Einstein and ROSAT were able to discover the ubiquitous occurrence of hot, tenuous coronae around late-type stars by detection of considerable X-ray luminosities for **all** late-type stars within the immediate neighborhood of the Sun (e.g., Schmitt 1997). The X-ray luminosity is a classical activity indicator and a relation between the X-ray luminosity and the rotational velocity $v \sin i$ (and thus age, e.g., Pallavicini et al. 1981) has been established. This suggests magnetic dynamo generation to be involved in the creation of stellar coronae and therefore also for the solar corona.

Common practice in analyzing X-ray spectra has been based on global fit approaches, putting all known aspects of the formation of X-ray spectra into a synthetic spectrum. The physical parameters (like plasma temperature) are then optimized in order to find best agreement between the synthetic spectrum and measured spectra. This method showed a general trend that plasma temperatures increase with increasing activity (Jordan & Montesinos 1991). Since the heating phenomena have still today not been discovered, this is an important contribution to some day approach a complete understanding of the formation and heating of stellar coronae and the solar corona.

In this spirit, the detailed physical description of stellar coronae is the next step in order to approach this aim. X-ray spectroscopy of the solar corona has been applied to measure temperatures and densities in specific active or quiescent regions. The solar corona was found to be essentially optically thin and the X-ray spectrum is thus dominated by emission lines. Important diagnostics tools have been developed, e.g., the density diagnostics with He-like triplets (Gabriel & Jordan 1969). All these tools can in principle also be applied to stellar coronae, however, very sensitive instruments are required in order to provide a decent spectral resolution. Also the results have to be interpreted with the limitation that only average coro-

nal properties can be obtained, because no spatial resolution is possible. The X-ray missions Chandra and XMM-Newton provide the ideal instrumental setup with their slitless grating spectrometers. With these gratings, spectra have been obtained in the last four years which clearly confirmed that the X-ray spectra of stellar coronae are also dominated by emission lines originating from highly ionized atomic transitions. Also continuum emission is found for more active stars, which is dominated by the bremsstrahlung mechanism (Ness et al. 2002). While the continuum reflects the plasma temperature of the hottest regions in the corona, the formation of each individual line reflects the physical conditions of the plasma regions emitting the respective lines. Since no individual emission regions can be isolated in a stellar corona the line diagnostics will return averages of all visible emission regions, weighted with the brightness of each region. This limitation implies that only typical properties of activity-related physical properties can be identified. When samples of stellar coronae are investigated, trends between coronal properties and stellar parameters can be discovered uncovering the underlying physical processes.

My paper will summarize all aspects of density analyses for stellar coronae. I will first give a short motivation indicating the diagnostic power available when densities are known. I will then give details how to measure densities and what the limitations of the methods are. A brief section for determining temperatures related to the measured densities will be included before I present typical structural information derived out of the densities and temperatures for a large sample of stellar coronae.

2. Motivation

The solar corona with its active regions is highly structured. This makes any attempts to construct exact models of stellar coronae futile. However, some scaling laws have been developed describing empirically how physical properties determine the sizes of coronal structures. The shape of most structures are loop-like following closed magnetic field lines. Semi-empirical loop-scaling laws have been developed by, e.g., Rosner et al. (1978), which are based on specific assumptions of a heating function (the heating per unit volume constant with temperature) and the boundary conditions on the conductive flux at the base and the top of a loop. They give

$$T_{\rm max} = 1.4 \times 10^3 (pL)^{1/3} \quad \text{or} \quad n_e L = 1.3 \times 10^6 T_{\rm max}^2 \qquad (1)$$

($T_{\rm max}$: loop-top temperature, p: electron pressure, n_e: electron density, L: semi-loop length) and good agreement with observations of solar active regions was reported. Better observations returned more refined scaling laws, but the basic principle is always the same: If temperatures and densities are derived, the semi-loop length L can be derived (under the assumption of constant pressure p along a loop).

The second relation combining geometrical and physical parameters is the definition of the volume emission measure

$$\mathrm{EM} = n_e n_H V \qquad (2)$$

(EM: Emission measure, n_e: electron density, $n_H = 0.85 n_e$: hydrogen density, and V: emitting volume). The emission measure specifies the amount of emitting material in the corona (units: cm^{-3}) and can directly be measured. A given emission measure can thus express either compact small emitting material or dense and large emission regions. In order to quantify the emission sizes one needs independent measurements of the electron density (under the assumption of cosmical composition, i.e., $n_H = 0.85 n_e$).

It is therefore instructive to measure densities and emission measures as well as temperatures and densities (specifically for the loop-top) in order to learn about emitting volumes and semi-loop lengths.

3. Methods

For the method it is important to first mention that all analyzes are made on the grounds of coronal equilibrium. This means that all excited states are populated by collisions exclusively. Here the number of collisions is not as important as their kinetic energy, i.e., the temperature of the plasma. Thus the formation of all lines is determined by their temperature-sensitive ionization balance and collisional cross sections. The energy stored in excited levels is assumed to generally be converted into radiative energy, and the de-excitations will emit the respective photons. An important assumption is that the plasma is effectively optically thin, i.e., no photons produced are scattered out of the line of sight. The general validity of this assumption has been tested by Ness et al. (2003b).

The basic method for measuring densities is based on the competition between radiative and collisional processes in depopulating an excited level. This requires a minimum time scale on which an excited level has to survive (metastable levels), to allow interactions with other excited levels. Such transitions are generally forbidden lines with low radiative de-excitation probabilities to the ground state. In practice line ratios are used, because ratios can be selected to isolate desired quantities from disturbing effects as, e.g., elemental abundances. If densities are to be determined at least one of the lines involved in the ratio has to be a forbidden line.

Popular density diagnostics used in the 1990s with EUVE data involved highly ionized iron lines, e.g., Fe XXI (Mason et al. 1979). The principle here is that excited levels with low radiative transition probabilities will be further excited by collisions into levels with higher radiative de-excitation probabilities and radiate down via that level. In the case of higher densities these alternative lines will show up in the spectrum and the detection of these

lines and increasing line strengths thus indicate significant densities. One example is the Fe XXI line at 102.35 Å which was analyzed by Dupree et al. (1993) in an EUVE spectrum of Capella. While they report unusually high densities based on the detection of the 102.35 Å and other lines (quantified by comparison with the reference line of Fe XXI at 128.78 Å), others, e.g., Schmitt et al. (1994) and Schmitt et al. (1996) find only low-density limits for Procyon and ϵ Eridani from the same lines. The densities reported by Dupree et al. (1993) imply that the 121.21 Å line is well detectable compared with the 128.73 Å line, but no reports on the detection of this line have ever been made for coronal plasmas.

The second method I would like to address involves the He-like triplets. This method was developed by Gabriel & Jordan (1969) and uses the ratio of two forbidden lines, namely an intercombination line, i ($^3P_1$–$^1S_0$), and a forbidden line, f ($^3S_1$–$^1S_0$). Interactions between the upper levels are of the kind that with increasing densities the upper level of the forbidden line will be depopulated exclusively in favor of the upper level of the intercombination line. This makes the ratio of the lines extremely sensitive to densities. Gabriel & Jordan (1969) have developed a parameterized form of the density-dependence of the f/i ratio with the two parameters low-density limit R_0 (the ratio of the radiative A coefficients) and the critical density N_c (where f/i drops to half of its low-density value):

$$\frac{\mathrm{f}}{\mathrm{i}} = \frac{R_0}{1 + n_e/N_c + \phi/\phi_c} \,. \qquad (3)$$

The term ϕ/ϕ_c accounts for competing radiative excitations of the transition $^3S_1$–$^3P_1$, which could be triggered by UV radiation from the stellar surface, but for most sources this term is negligible (for more details see Ness et al. 2002). The parameters differ from ion to ion only due to their nuclear charge Z. This leads to decreasing low-density limits R_0 and increasing critical densities N_c with increasing nuclear charge (power-law). This is illustrated with Fig. 1. On the top axis the peak formation temperatures T_M of the respective ions are also plotted. The figure demonstrates that in hotter plasmas $T > 6$ MK densities $\sim 10^{10}\,\mathrm{cm}^{-3}$ will not be measurable and the diagnostics will instead return low-density limits. The Fe XXI diagnostics are sensitive at lower densities in the high temperature regime, but densities as low as $10^{10}\,\mathrm{cm}^{-3}$ will also not be measurable with the Fe XXI diagnostics. The density dependence of the He-like f/i ratio has also been modeled theoretically (e.g., Porquet et al. 2001) and it is also listed in the Chianti and APEC databases. Within the expected measurement errors the parameterized form Eq. 3 performs sufficiently well compared to the different other compilations in order to be used for quantitative density measurements (Ness et al. 2004).

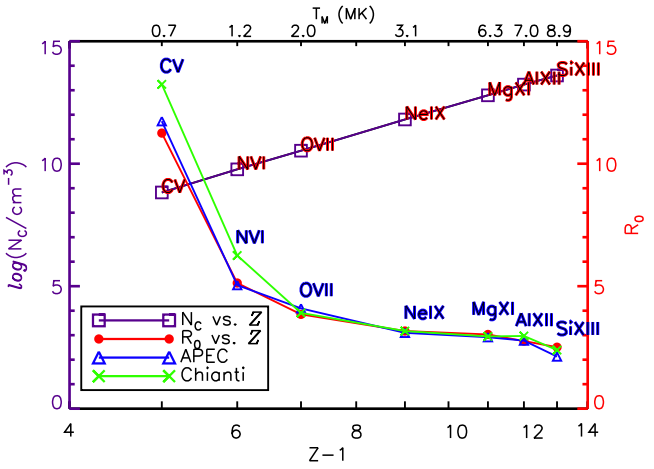

Figure 1. Values of parameters N_c (left axis) and R_0 (right axis) in Eq. 3 as a function of nuclear charge Z-1 (screened by one electron). Values are from Blumenthal et al. (1972) and the low-density limits are compared with Chianti and APEC values. Peak formation temperatures of the ions, T_M, are given in the top.

3.1. Temperatures associated with densities

According to Eq. 1 in Sect. 2 temperatures are needed in addition to the densities in order to understand the structures of stellar coronae. Since all diagnostics refer only to an average of all emitting regions, a temperature diagnostic is desired which refers directly to those regions which the densities refer to. An ideal way to estimate temperatures on the same average level is the additional use of the H-like line of the same element, e.g., the O VII He-like triplet for the densities and the O VIII Ly$_\alpha$ line for the temperature. The temperature is then determined by comparison of the ratio of the O VII resonance line r ($^1P_1$–$^1S_0$) with the O VIII H-like line with theoretical ratios. Fig. 2 shows the H-like to He-like theoretical predictions for several pairs of ions with measurements of some stars (Algol, Capella, ϵ Eri, and Procyon). It can be seen that the shape of the temperature distribution can be recognized yielding a cool corona for Procyon and the hottest corona for Algol. Note that each individual line ratio is independent of the elemental abundance.

4. Measurement of densities

4.1. Direct measurements

Since stellar coronae are all point-like sources, no direct measurements of structures are possible with the present angular resolution. However, in some rare exceptions of eclipsing binaries the structures of the emitting plasma can be reconstructed from the X-ray light curve if one component is completely X-ray dark (e.g., Schmitt 1996). One such example is Algol, where the optical primary is X-ray dark (e.g., Chung et al. 2004). With the orbital

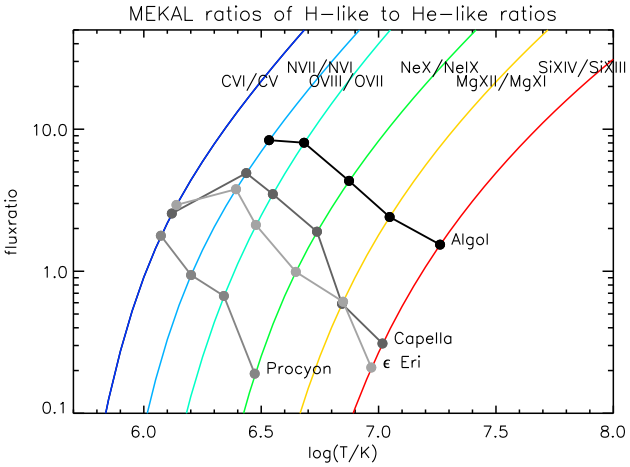

Figure 2. Temperature-sensitive line ratios associated with the He-like density diagnostics.

period of 2.8 days this target can be observed with reasonable exposure times concentrating on either (optical) primary or secondary minimum. Such observations were carried out with all past X-ray missions concentrating on the secondary minimum, i.e., when the X-ray active component was to be eclipsed by the primary. While the quiescent emission appears not to be affected by the eclipse (e.g., White et al. 1986; although Ottmann & Schmitt 1996 did see evidence for a partial eclipse), more local phenomena as flares can well be eclipsed opening the opportunity of studies of the spatial distribution of the flaring plasma. Such flares were observed with EXOSAT by Schmitt & Favata (1999) and recently with XMM-Newton by Schmitt et al. (2004). The reconstruction of the spatial intensity distribution of the flare was carried out according to Schmitt (1996) and is shown in the left panel of Fig. 3. One can also study the density in the flare using Eq. 2. In this way Schmitt et al. (2004) found that more than 70% of the emission resides at densities higher than $10^{11}\,\mathrm{cm}^{-3}$, which is consistent with the simultaneously obtained spectroscopic density (from RGS). Another such system is α CrB, where Schmitt & Kürster (1993) found a total eclipse in X-rays, proving that the A-type star is X-ray dark. With a recent XMM-observation Güdel et al. (2003); Güdel (2004) reconstructed the emission structure of the eclipsed plasma, and it was possible to construct an emission measure map (Fig. 3; right). In the same fashion as Schmitt et al. (2004) a density map was derived from the combined spatial and intensity information.

However, these systems are rare exceptions and do not necessarily represent stellar coronae in general (otherwise the study of the solar corona would be sufficient). In cases were no direct measurements are possible, spectroscopic methods usually fill the gap.

4.2. He-like triplets

Since the X-ray grating spectra have such a high resolution, each spectral bin contains only a small number of counts. The spectral fitting thus requires special treatment in order not to ruin the statistics. This problem has been addressed by Cash (1979) who proposed a maximum likelihood estimation in order to fit spectral models to low-count spectra. The criterion demands that traditional χ^2 statistics can only be applied if **all** spectral bins contain at least 15 counts. Since this is not the case for Chandra and XMM-Newton grating spectra it is necessary to use maximum likelihood fitting. The alternative would be to rebin until all bins contain more than 15 counts, but this would mean that the excellent spectral resolution is thrown away before the analysis even started. A program systematically pursuing this philosophy is the CORA program by Ness & Wichmann (2002b), so I use it in order to obtain all line counts required to do the density and temperature analyses. The spectral model of a line template is an analytic line profile approximating the instrumental line profile. These are Lorentzians for the RGS spectra and modified Lorentzians (β profiles according to Drake 2003 with $\beta = 2.4$) for the Chandra grating spectra. These modified Lorentzians are nearly Gaussians. The line widths are always fixed to the instrumental line widths (RGS and LETGS: 0.06 Å, MEG: 0.01 Å, and HEG: 0.005 Å). The line counts obtained for the O VII and Ne IX f and i lines are listed in Tables 1 and 2 and f/i ratios were calculated accounting for the effective areas extracted with the SAS and CIAO software packages. (These values are also published in the electronic version of Ness et al. 2004, but are only printed here). Densities derived from Eq. 3 are also listed with parameters $R_0 = 3.95$ and $N_c = 3.1 \times 10^{10}\,\mathrm{cm}^{-3}$ for O VII and $R_0 = 3.4$ and $N_c = 5.9 \times 10^{11}\,\mathrm{cm}^{-3}$ for Ne IX (Blumenthal et al. 1972; see also Fig. 1). It can be seen that the densities obtained from the Ne IX triplet come out systematically higher. Since Ne IX represents higher temperatures, this implies, that the two ions represent different plasma regions with different pressures. However, this could in principle be an artifact from the complicated blending structure of the Ne IX triplet region (Ness et al. 2003a). This complicated blending is the reason why only MEG and HEG data were analyzed, but no LETGS and RGS data. Nevertheless, Ness et al. (2003a) found that even with the best resolution of the HEG, an unresolved blend with the intercombination line of Ne IX is possible. Ness et al. (2004) carried out an analysis estimating the blending flux and found that this effect cannot fully account for the systematically higher densities. A similar work focusing on the Mg XI and Si XIII triplets has been presented by Testa et al. (2004). They attempt to disentangle complicated blending of the Mg XI triplet lines by high-n H-like Ne X lines. They found mostly low-density limits, but also some significant deviations from the low-density limit. The Mg XI f/i ratios appear to correlate with

the ratio of $L_X/L_{\rm bol}$, but not with the surface flux F_X. They measured Si XIII f/i ratios, which were systematically higher than the theoretical low-density limit. They explain this by uncertainties in the theoretical ratios, but such an effect is not discussed for the theoretical Mg XI low-density limits. Also, the effects of low-temperature dielectronic satellite lines can be very strong for high-Z ions. These lines can be blended either with the intercombination line or the forbidden line or both, and ignoring this blending can lead to incorrect densities. The fluxes of dielectronic satellite lines are negligible for the oxygen and neon He-like triplets in coronal plasmas.

4.3. Fe XXI line ratios

The measurement of several Fe XXI lines has been possible with, e.g., EUVE. Some of these lines can now be remeasured with the LETGS aboard Chandra (wavelength range up to 175 Å). The density-sensitive lines of Fe XXI are by their nature complementary to the He-like triplet, because they probe the hotter plasma regions at lower densities than He-like Si XIII and Mg XI f/i ratios. Dupree et al. (1993) have analyzed Fe XXI lines at 102.35 Å, 142.15 Å, 145.65 Å, and 128.73 Å for density estimates and find densities $4 \times 10^{11} - 10^{13}\,{\rm cm}^{-3}$. Mewe et al. (2001) reanalyzed some of these lines and included more line ratios, also from Fe XX and Fe XXII, but report only densities below $2 \times 10^{12}\,{\rm cm}^{-3}$. A systematic comparison of the EUVE measurements and the LETGS data is presented by Ness et al. (2004). Their Fig. 5 clearly shows that the line ratios reported by Dupree et al. (1993) are not consistent with the LETGS data and that the 121.21 Å, 142.16 Å, and 145.65 Å lines are significantly weaker compared to the 128.73 Å line. This is in line with other EUVE results (e.g., Schmitt et al. 1994; Schmitt et al. 1996), where only low densities were found for Procyon and ϵ Eri. However, more recent analyzes of AB Dor by Sanz-Forcada et al. (2003) using the HETGS aboard Chandra, again, returned individual high densities. They used high-energy (10 Å – 12 Å) lines of highly ionized iron and found some high densities, but at the same time low-density limits from different line ratios of the same ion. Since all lines measured from a given ion must originate from the same plasma regions they should all return the same densities. In pathologic cases, however, a local high-density region could contribute to high-density lines, while a large number of low-density regions contribute all to the low-density lines, such that the density diagnostics return only a weighted average of these densities. High-density lines formed more efficiently might thus be stronger in a spectrum obtained for the complete corona of such a scenario than other high-density lines leading to supposedly contrary results.

The main problem with the Fe densities is that the density diagnostics rely on the detection of strategic lines. Reliable densities can only be expected if **all** blending lines in the respective wavelength regions were known. Although the atomic databases have made great progress in the recent past, unrecognized lines can still not fully be excluded at any given wavelength. If different density diagnostics from the same ion result in different densities, the lowest densities returned have to be most trusted, because any high densities formally derived can in principle be due to overestimated line fluxes, while underestimated line fluxes are unlikely.

5. Discussion

For the understanding of coronal structures in stellar coronae direct measurements give us only limited access via eclipses in rare examples. Two of those are plotted in Fig. 3 and it can be seen that the X-ray coronae of other stars are just as highly structured as the solar corona is. Also, the assumption of loop-like structures appears to be reasonable. For all the other stars spectroscopic temperature- and density measurements allow structural information to be obtained with some simplifying assumptions. These are in particular, that the building blocks are loop-like structures that obey a given scaling law, e.g., Rosner et al. (1978). The second assumption is that a distribution of loop-like structures is present, e.g., a uniform distribution with all identical loops. Such a distribution cannot be reconstructed and has to be assumed.

In order to demonstrate how this works in principle I will now assume all stellar coronae in the sample of density measurements to be composed of identical standard loops, whose properties will have to be evaluated from scaling laws. For simplicity Ness et al. (2004) assumed that these loops are constant-pressure loops obeying the Rosner et al. (1978) scaling law (Eq. 1). Density and temperature measurements allow one to estimate the semi-loop length, which can be regarded as the extent of the coronal plasma above the stellar surface. However, for the application of Eq. 1 one needs the loop-top conditions, which are not necessarily probed with the He-like density analyses. In fact, with the O VII triplet only the cooler plasma components are probed rather than the hottest loop-top conditions. The Ne IX triplet is more representative, but for the hottest coronae, even those temperatures (~ 4 MK) do not represent the loop-top conditions. One could still use densities and temperatures derived from H-like/He-like line ratios, however, one will then always underestimate the loop lengths, which will give a lower limit to the extent of the corona.

Another way of deriving more realistic scale heights is to estimate a loop-top temperature from the activity of stars (in terms of L_X). Güdel et al. (1997) analyzed a sample of nine solar-like stars and found that the hottest temperature component scales with the X-ray luminosity. Since in the sample of densities all kinds of stars are present, it is better to use surface X-ray fluxes and thus

$$T_{\rm hot}^4 = \frac{L_X}{55} \left(\frac{R_\star}{R_\odot} \right)^{-2} . \qquad (4)$$

Table 1. Measured line counts for O VII and Ne IX intercombination (i) and forbidden (f) lines, corresponding f/i ratios (corrected for $A_{\rm eff}$), and plasma densities n_e derived from Eq. 3. All errors are $1\,\sigma$ errors.

		O VII				Ne IX			
star	Instr.	i [cts]	f [cts]	f/i	log(n_e)	i [cts]	f [cts]	f/i	log(n_e)
24 UMa	MEG	2.55 ± 1.97	14.52 ± 4.00	6.37 ± 5.22	< 11.9	18.84 ± 5.70	80.49 ± 10.10	4.69 ± 1.53	< 11.8
	HEG	–	–	–	–	8.83 ± 3.32	13.64 ± 3.99	1.61 ± 0.77	11.8 ± 0.42
44 Boo	MEG	32.92 ± 6.46	49.79 ± 7.70	1.69 ± 0.42	10.6 ± 0.19	132.90 ± 15.01	352.56 ± 25.21	2.91 ± 0.39	11.0 ± 0.52
	HEG	–	–	–	–	40.76 ± 7.17	84.48 ± 10.46	2.17 ± 0.47	11.5 ± 0.27
47 Cas	RGS1	55.19 ± 12.64	105.41 ± 14.67	2.00 ± 0.54	10.5 ± 0.24	–	–	–	–
AB Dor	RGS1	230.94 ± 24.70	407.50 ± 27.21	1.83 ± 0.23	10.5 ± 0.10	–	–	–	–
	MEG	15.60 ± 5.02	36.98 ± 6.75	2.65 ± 0.98	10.2 ± 0.74	137.61 ± 13.53	290.84 ± 18.73	2.32 ± 0.27	11.4 ± 0.16
	HEG	–	–	–	–	33.50 ± 6.11	77.68 ± 9.19	2.42 ± 0.53	11.4 ± 0.37
α Cen A	LETG	38.41 ± 6.99	109.60 ± 11.06	2.82 ± 0.59	10.1 ± 0.39	–	–	–	–
α Cen B	RGS1	20.34 ± 6.49	111.23 ± 11.60	5.68 ± 1.91	< 10.2	–	–	–	–
	LETG	36.09 ± 7.09	154.54 ± 13.06	4.23 ± 0.90	< 10.8	–	–	–	–
AD Leo	RGS1	166.09 ± 17.75	356.13 ± 22.02	2.23 ± 0.27	10.4 ± 0.12	–	–	–	–
	LETG	53.01 ± 9.21	170.31 ± 14.52	3.17 ± 0.61	9.92 ± 0.74	–	–	–	–
	MEG	18.56 ± 4.45	30.68 ± 5.65	1.85 ± 0.56	10.5 ± 0.25	53.71 ± 7.85	171.40 ± 14.05	3.50 ± 0.59	< 12.0
	HEG	–	–	–	–	12.77 ± 3.61	26.91 ± 5.26	2.20 ± 0.76	11.5 ± 0.50
Algol	RGS1	104.99 ± 25.25	90.89 ± 24.58	0.90 ± 0.33	10.6 ± 1.41	–	–	–	–
	LETG	186.85 ± 22.27	184.01 ± 22.30	0.97 ± 0.17	10.4 ± 0.47	–	–	–	–
	MEG	51.46 ± 8.54	31.58 ± 7.29	0.69 ± 0.19	10.9 ± 0.29	150.82 ± 15.43	236.96 ± 18.28	1.72 ± 0.22	11.7 ± 0.11
	HEG	–	–	–	–	35.73 ± 6.99	53.05 ± 8.12	1.55 ± 0.39	11.8 ± 0.20
AT Mic	RGS1	134.91 ± 17.58	238.57 ± 18.83	1.84 ± 0.28	10.5 ± 0.12	–	–	–	–
AU Mic	RGS1	209.47 ± 21.95	688.37 ± 31.28	3.44 ± 0.39	9.70 ± 0.67	–	–	–	–
	MEG	10.05 ± 3.52	45.99 ± 6.97	5.11 ± 1.95	< 10.9	78.25 ± 9.95	214.19 ± 15.80	3.00 ± 0.44	10.9 ± 1.00
	HEG	–	–	–	–	24.99 ± 5.08	52.33 ± 7.29	2.19 ± 0.54	11.5 ± 0.32
β Cet	RGS1	19.48 ± 8.40	79.44 ± 11.74	4.23 ± 1.93	< 11.3	–	–	–	–
	LETG	58.12 ± 16.27	178.69 ± 20.17	3.03 ± 0.92	< 11.0	–	–	–	–
	MEG	5.49 ± 3.00	23.61 ± 5.25	4.80 ± 2.83	< 11.5	127.79 ± 14.00	211.92 ± 17.14	1.82 ± 0.25	11.7 ± 0.12
	HEG	–	–	–	–	32.41 ± 6.07	64.72 ± 8.30	2.09 ± 0.47	11.6 ± 0.26
Canopus	MEG	1.20 ± 1.41	13.42 ± 3.87	12.47 ± 15.09	–	23.29 ± 5.74	42.20 ± 7.13	1.99 ± 0.59	11.6 ± 0.33
	HEG	–	–	–	–	4.68 ± 2.28	13.03 ± 3.66	2.91 ± 1.64	< 12.0
χ^1 Ori	RGS1	22.27 ± 8.18	123.42 ± 13.40	5.75 ± 2.20	< 10.5	–	–	–	–
EK Dra	RGS1	30.25 ± 8.06	59.68 ± 9.82	2.05 ± 0.64	10.4 ± 0.29	–	–	–	–
	LETG	23.82 ± 7.19	31.03 ± 7.53	1.29 ± 0.50	10.8 ± 0.28	–	–	–	–
ϵ Eri	RGS1	41.69 ± 8.90	160.21 ± 14.34	3.99 ± 0.92	< 10.9	–	–	–	–
	LETG	153.61 ± 14.85	453.99 ± 22.78	2.92 ± 0.32	10.0 ± 0.20	–	–	–	–
EQ Peg	RGS1	46.25 ± 9.95	142.72 ± 13.99	3.20 ± 0.76	< 10.8	–	–	–	–
ER Vul	MEG	4.14 ± 3.03	18.06 ± 5.05	4.88 ± 3.83	< 11.9	51.41 ± 9.56	168.72 ± 14.75	3.60 ± 0.74	< 12.1
	HEG	–	–	–	–	16.96 ± 4.53	32.71 ± 6.17	2.02 ± 0.66	11.6 ± 0.37
EV Lac	RGS1	128.92 ± 16.34	291.00 ± 20.31	2.34 ± 0.34	10.3 ± 0.16	–	–	–	–
	MEG	40.31 ± 6.59	54.92 ± 7.58	1.52 ± 0.33	10.7 ± 0.15	85.95 ± 10.78	222.32 ± 16.34	2.84 ± 0.41	11.1 ± 0.48
	HEG	–	–	–	–	24.32 ± 5.20	68.82 ± 8.55	2.96 ± 0.73	< 12.0
HD 223460	MEG	10.64 ± 3.89	7.37 ± 3.36	0.77 ± 0.45	11.1 ± 0.43	–	–	–	–
κ Cet	RGS1	63.15 ± 11.60	153.99 ± 15.00	2.55 ± 0.53	10.2 ± 0.28	–	–	–	–
μ Vel	MEG	4.26 ± 2.96	27.60 ± 5.73	7.24 ± 5.24	< 11.5	50.20 ± 8.94	59.62 ± 9.23	1.30 ± 0.31	11.9 ± 0.17
	HEG	–	–	–	–	24.12 ± 5.49	31.65 ± 5.93	1.37 ± 0.40	11.9 ± 0.22
π^1 UMa	RGS1	30.39 ± 8.22	94.81 ± 11.76	3.24 ± 0.96	< 10.8	–	–	–	–
Procyon	LETG	203.00 ± 16.80	652.40 ± 27.40	3.17 ± 0.29	9.90 ± 0.25	–	–	–	–
Prox Cen	MEG	5.73 ± 2.45	18.19 ± 4.33	3.55 ± 1.74	< 10.5	5.54 ± 2.89	18.02 ± 5.03	3.57 ± 2.11	< 12.9
	HEG	–	–	–	–	2.93 ± 1.73	12.81 ± 4.92	4.57 ± 3.22	< 12.9
Speedy Mic	MEG	3.75 ± 2.22	8.56 ± 3.14	2.55 ± 1.77	< 11.2	11.57 ± 3.68	37.35 ± 6.82	3.54 ± 1.30	< 12.5
	HEG	–	–	–	–	2.77 ± 1.74	10.59 ± 3.32	3.99 ± 2.80	< 13.0
V471 Tau	LETG	16.11 ± 7.37	43.43 ± 9.19	2.66 ± 1.34	< 11.2	–	–	–	–
VW Cep	LETG	72.06 ± 12.18	89.71 ± 12.90	1.23 ± 0.27	10.8 ± 0.15	–	–	–	–
ξ UMa	MEG	39.15 ± 6.40	72.85 ± 8.65	2.08 ± 0.42	10.4 ± 0.19	138.57 ± 13.41	354.90 ± 20.13	2.81 ± 0.32	11.1 ± 0.31
	HEG	–	–	–	–	29.59 ± 5.73	81.17 ± 9.20	2.87 ± 0.64	< 12.1
YY Gem	LETG	50.64 ± 9.63	115.75 ± 12.44	2.26 ± 0.49	10.4 ± 0.23	–	–	–	–
YZ CMi	RGS1	88.70 ± 13.07	169.54 ± 15.80	2.00 ± 0.35	10.5 ± 0.15	–	–	–	–

The density at the loop-top can then be calculated from assuming constant pressure along the loop. From the semi loop length L (when assumed to represent the extent of the coronal plasma) it is possible to calculate a volume which can potentially be filled with X-ray emitting plasma by multiplying with the stellar surface

$$V_{\rm avail} = 4\pi R_\star^2 L_{\rm loop} \,. \qquad (5)$$

(Terms of L^2 and L^3 are here neglected against the stellar radius). In Fig. 4 I compare the available volumes obtained when using the temperatures from the H-like to He-like line ratios and using the temperatures obtained when scaling with the X-ray luminosity according to Eq. 4. Obviously the volumes come out significantly larger with the approach using higher temperatures, also for the cooler coronae. The degree of activity is marked by different sym-

Table 2. Same as Table 1 for RS CVn systems in the sample.

		O VII				Ne IX			
star	Instr.	i [cts]	f [cts]	f/i	log(n_e)	i [cts]	f [cts]	f/i	log(n_e)
AR Lac	RGS1	48.70 ± 14.75	110.15 ± 16.82	2.35 ± 0.80	10.3 ± 0.42	–	–	–	–
	MEG	1.60 ± 2.58	3.80 ± 2.86	2.65 ± 4.71	–	48.98 ± 8.38	140.80 ± 13.32	3.15 ± 0.62	< 11.8
	HEG	–	–	–	–	10.09 ± 3.67	13.90 ± 4.23	1.44 ± 0.68	11.9 ± 0.40
Capella	RGS1	339.67 ± 30.84	1618.64 ± 48.15	4.95 ± 0.47	–	–	–	–	–
	LETG	645.44 ± 33.14	2348.32 ± 53.78	3.59 ± 0.20	9.51 ± 0.40	–	–	–	–
	MEG	167.92 ± 13.94	505.48 ± 23.16	3.36 ± 0.32	9.76 ± 0.38	709.92 ± 32.20	1373.17 ± 42.87	2.12 ± 0.12	11.5 ± 0.06
	HEG	–	–	–	–	190.47 ± 14.76	373.48 ± 20.09	2.05 ± 0.19	11.6 ± 0.10
HR 1099	RGS1	82.61 ± 19.30	254.27 ± 23.89	3.20 ± 0.80	< 10.9	–	–	–	–
	LETG	114.78 ± 18.72	254.79 ± 22.49	2.19 ± 0.41	10.4 ± 0.18	–	–	–	–
	MEG	36.05 ± 8.90	93.87 ± 11.80	2.91 ± 0.81	10.0 ± 0.75	304.42 ± 24.39	834.17 ± 34.81	3.01 ± 0.27	10.9 ± 0.38
	HEG	–	–	–	–	100.55 ± 11.62	228.75 ± 16.25	2.38 ± 0.32	11.4 ± 0.20
II Peg	MEG	33.61 ± 6.95	44.83 ± 7.82	1.49 ± 0.40	10.7 ± 0.20	103.95 ± 13.27	268.87 ± 18.85	2.84 ± 0.41	11.1 ± 0.48
	HEG	–	–	–	–	19.99 ± 4.55	46.00 ± 6.95	2.41 ± 0.66	11.4 ± 0.50
IM Peg	MEG	4.46 ± 3.49	10.70 ± 4.16	2.68 ± 2.34	< 11.2	49.64 ± 9.16	127.99 ± 13.33	2.83 ± 0.60	11.1 ± 1.05
	HEG	–	–	–	–	12.86 ± 4.01	30.64 ± 5.83	2.49 ± 0.91	11.3 ± 1.14
λ And	RGS1	39.10 ± 15.08	131.08 ± 17.88	3.48 ± 1.42	< 10.6	–	–	–	–
	LETG	72.16 ± 21.57	259.98 ± 26.03	3.56 ± 1.12	< 10.5	–	–	–	–
	MEG	11.47 ± 4.64	33.55 ± 6.64	3.27 ± 1.47	< 10.8	81.33 ± 11.89	219.34 ± 17.80	2.96 ± 0.49	11.0 ± 1.12
	HEG	–	–	–	–	12.84 ± 3.92	35.64 ± 6.22	2.90 ± 1.02	< 12.0
σ^2 CrB	RGS1	61.46 ± 15.44	173.44 ± 20.53	2.93 ± 0.81	10.0 ± 0.80	–	–	–	–
	MEG	50.90 ± 7.91	94.28 ± 10.29	2.07 ± 0.39	10.4 ± 0.17	296.10 ± 20.73	521.80 ± 26.92	1.93 ± 0.17	11.6 ± 0.08
	HEG	–	–	–	–	88.11 ± 9.85	130.60 ± 11.74	1.55 ± 0.22	11.8 ± 0.11
TY Pyx	MEG	6.52 ± 2.82	7.52 ± 2.98	1.29 ± 0.76	10.8 ± 0.49	26.51 ± 7.03	72.69 ± 9.73	3.01 ± 0.89	< 11.9
	HEG	–	–	–	–	7.09 ± 3.13	16.96 ± 4.54	2.50 ± 1.29	< 12.3
UX Ari	RGS1	30.31 ± 15.89	117.54 ± 18.79	4.03 ± 2.21	< 11.5	–	–	–	–
	LETG	53.55 ± 14.68	227.42 ± 20.40	4.19 ± 1.21	< 11.0	–	–	–	–
	MEG	7.02 ± 3.76	20.91 ± 5.42	3.33 ± 1.98	< 10.8	120.16 ± 12.36	237.38 ± 17.32	2.17 ± 0.27	11.5 ± 0.15
	HEG	–	–	–	–	7.99 ± 3.23	18.57 ± 4.60	2.43 ± 1.15	< 12.4
V824 Ara	MEG	22.35 ± 5.24	30.23 ± 6.02	1.51 ± 0.46	10.7 ± 0.23	157.09 ± 15.50	298.00 ± 19.26	2.08 ± 0.25	11.6 ± 0.13
	HEG	–	–	–	–	29.84 ± 5.90	66.01 ± 8.44	2.31 ± 0.54	11.4 ± 0.35
VY Ari	RGS1	52.58 ± 14.52	144.81 ± 17.34	2.86 ± 0.86	10.1 ± 0.79	–	–	–	–

bols in different colors (L_X refers here to the line fluxes in the He-like lines r+i+f, converted to luminosities). Also it can be noticed that the agreement of volumes is better for the Ne analysis, because Ne is formed at temperatures which are closer to the loop-top. With Mg the situation improves even better.

Now where the volumes available to X-ray emitting plasma have been calculated, it is instructive to see how much of this volume is actually filled with coronal plasma. This can simply be estimated by calculating emission volumes from Eq. 2. At this point, again, the densities measured with the He-like f/i ratios enter the stage. The emission measure EM in Eq. 2 is calculated by dividing the luminosity in all He-like triplet lines (r+i+f) by the peak emissivity of the lines extracted from the APEC database (thus assuming an isothermal plasma at the peak formation temperature, which is justified from the narrow temperature formation range of the He-like lines). The ratio of this emission volume and the available volume defines a volume filling factor, expressing the fraction of volume filled with coronal plasma. These calculations have been carried out by Ness et al. (2004) and they found the volume filling factors to be relatively constant for the O VII emitting plasma, while a significant increase in filling factors towards higher activity was detected for the (hotter) Ne IX emitting plasma (see Fig. 5). Such an increase was also found by Testa et al. (2004) for Mg XI emitting plasma using surface filling factors.

6. Summary and Conclusions

The measurement of electron densities is crucial for deriving structural information for stellar coronae not belonging to the useful class of eclipsing binaries with an X-ray dark and an X-ray bright component. These densities can be inferred from He-like triplets measured in the grating spectra obtained with Chandra and XMM-Newton. The densities we are dealing with in stellar coronae, however, are in a surprisingly low range, not exceeding $\log n_e = 12.5$ (Ness et al. 2004). Although five He-like ions are available in the wavelength ranges, only O VII and Ne IX can be used. The carbon (C V) and nitrogen (N VI) lines are too faint and are only effectively formed in the coolest stars, and Mg XI and Si XIII measure at extremely high densities that are rather the exception than the rule in stellar coronae (Testa et al. 2004). The Fe XXI line diagnostics are much more promising in order to probe the hotter plasma. The density-sensitive line ratios start deviating from their low-density limit at densities above $\log n_e = 11.5$, and the lines are formed at temperatures up to 10 MK. However, it appears that these line ratios cannot constrain any densities due to their specific problems. The diagnostics are biased to measure higher densities and all past claims of densities exceeding $\log n_e = 12.5$ (e.g., Dupree et al. 1993; Sanz-Forcada et al. 2003) were not consistent with simultaneous measurements of lower densities with lines from the same ions. Also, Testa et al. (2004) expected to

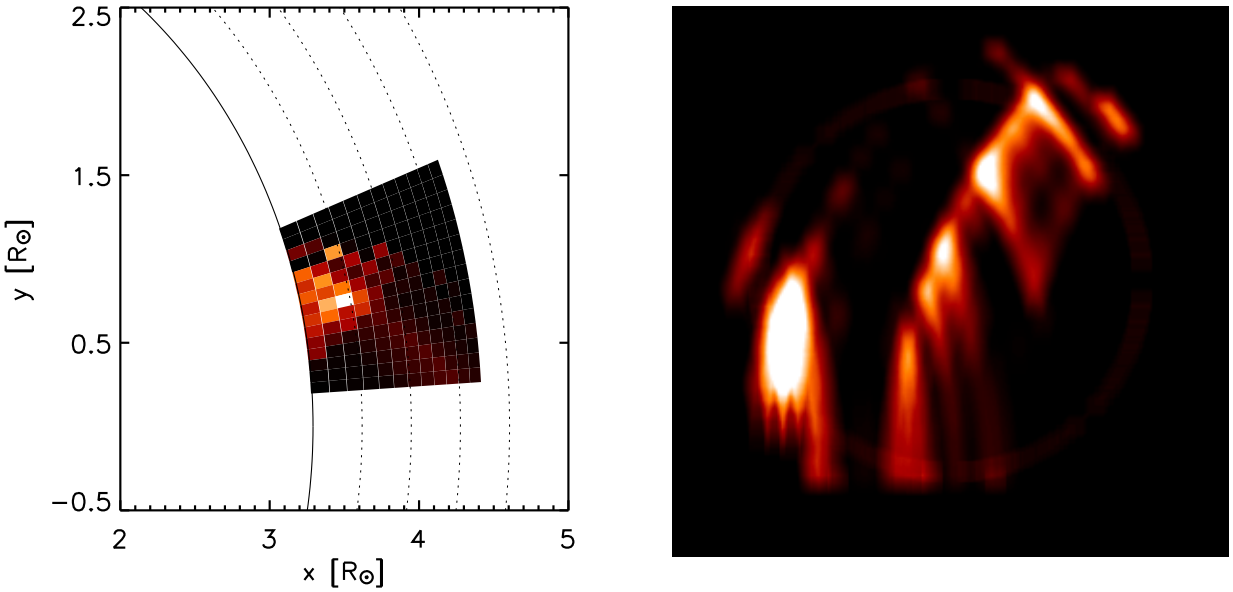

Figure 3. Reconstruction of stellar coronal plasma from eclipse studies for the examples of Algol (left panel: Schmitt et al. 2004) and α CrB (right panel: Güdel 2004).

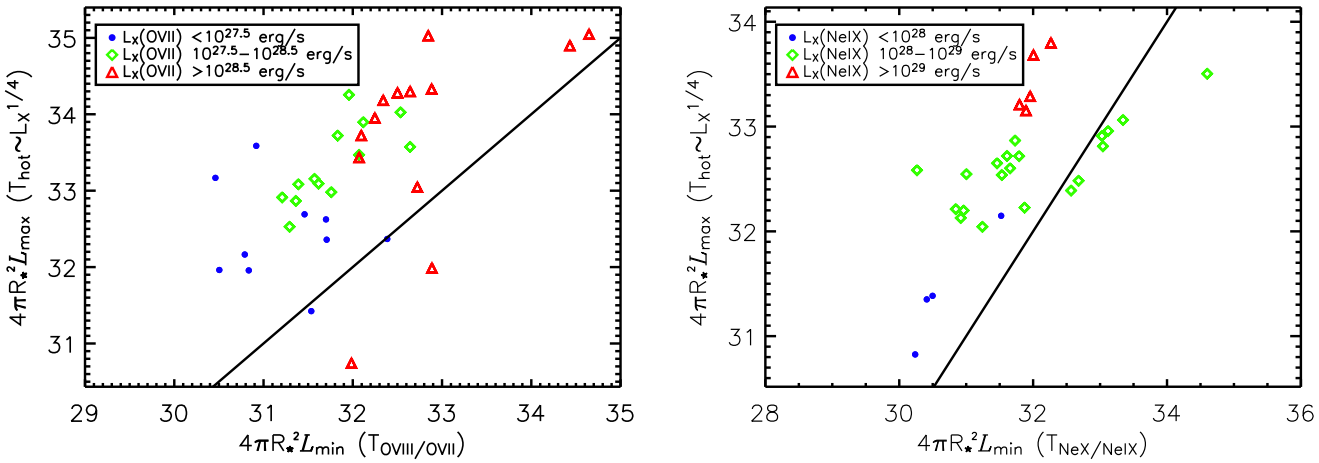

Figure 4. Comparison of coronal extent times stellar surface obtained from Eq. 1 with temperatures from the H-like to He-like line ratios (→ $L_{\rm min}$) and from the scaling equation 4 (→ $L_{\rm max}$). Left panel: O VII, right panel: Ne IX.

see clearer evidence for higher densities from their Mg XI triplets, referring to previous claims of high densities derived from the Fe lines. Therefore, the only constrained densities presently available have been measured with the He-like triplets of oxygen and neon.

While the hottest plasma regions cannot be probed at present, the cooler plasma regions still deliver useful information. The O VII f/i ratios returned many low-density limits, but also some constraints on plasma densities, which are all in the range $10^{10}-10^{11}\,{\rm cm}^{-3}$. These densities apply to plasma regions of temperatures around 2×10^6 K. This implies pressures $p=2n_ekT$ up to $60\,{\rm dyn/cm}^2$. The Ne IX f/i ratios return systematically higher densities $10^{11}-10^{12}\,{\rm cm}^{-3}$, and the lines are formed in plasma with temperatures 4×10^6 K. This implies pressures up to 1000 dyn/cm^2, so more than an order of magnitude higher pressures. With the assumption of constant pressure loops we are obviously not observing the same types of loops with the two density diagnostics, but rather different parts of a distribution of constant-pressure loops. The volume filling factors calculated from the two different density diagnostics (Fig. 5) shows different behavior with increasing activity. While the O VII emitting material fills available volume always with a similar percentage, the material dom-

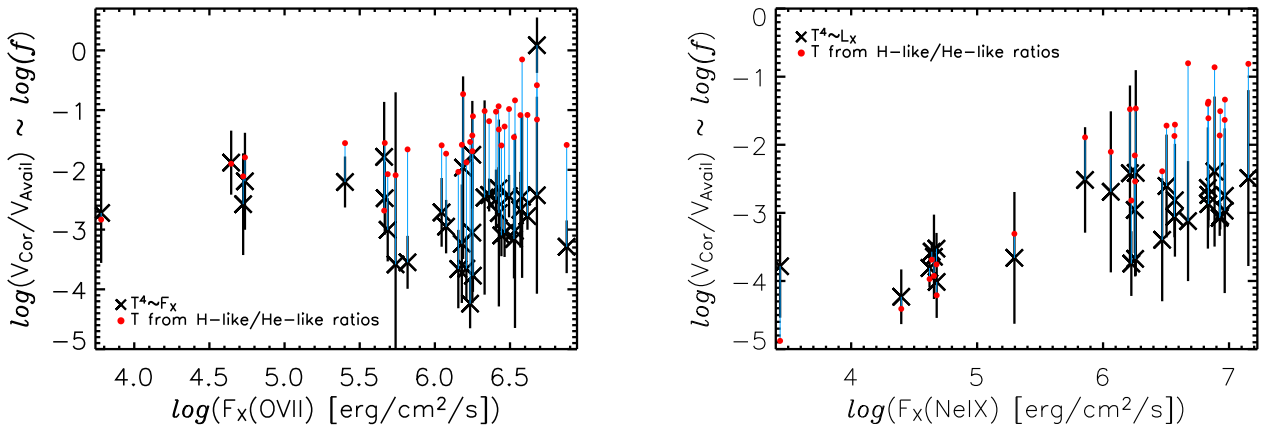

Figure 5. Filling factors obtained from ratios of coronal volumes (derived from O VII *and Ne* IX *densities) and assumed available volumes. The latter depend on assumed loop-top temperatures, which were derived from the H-like and He-like line ratios (marked with red bullets) and from L_X (Eq. 4). As activity indicator the surface fluxes F_X from $L_X(\mathrm{ion})/(4\pi R_*^2)$ are used.*

inating the Ne IX emission fills available volume considerably more efficient with increasing activity. The population with high-pressure loops will therefore increase for the more active stars, while less than 0.01 % of the volume in inactive stars will contain high-pressure loops. This trend has also been found by Testa et al. (2004) with their analysis for Mg XI emitting material, although due to a large number of low-density limits, their sample of constrained densities is quite small (they assumed $2 \times 10^{10}\,\mathrm{cm}^{-3}$ in the place of low-density limits).

These results are based on the application of the Rosner et al. (1978) scaling law, and so depend on the particular assumptions made there. However, this study primarily focuses on the density measurements and the method in principle. Many interesting approaches of scaling laws can now be applied with the densities obtained from the Chandra and XMM-Newton measurements.

Acknowledgements

I thank Prof. Carole Jordan for inspiring discussion about the paper. I acknowledge financial support from Deutsches Zentrum für Luft- und Raumfahrt e.V. (DLR) under 50OR98010.

References

Blumenthal, G.R., Drake, G.W., & Tucker, W.H. 1972, ApJ 172, 205
Cash, W. 1979, ApJ 228, 939
Chung, S.M., Drake, J.J., Kashyap, et al. 2004, ApJ 606, 1184
Drake, J.J. 2003, Chandra News 9, 14
Dupree, A.K., Brickhouse, N.S., Doschek, G.A., et al. 1993, ApJ 418, L41
Edlén, B. 1943, Zeitschrift für Astrophysik 22, 30
Gabriel, A.H. & Jordan, C. 1969, MNRAS 145, 241
Grotrian, W. 1931, Zeitschrift für Astrophysics 3, 199
Grotrian, W. 1939, Naturwiss. 27, 214
Güdel, M., Guinan, E.F., & Skinner, S.L. 1997, ApJ 483, 947
Güdel, M., Arzner, K., Audard, M., & Mewe, R. 2003, A&A 403, 155
Güdel, M. 2004, A&A Reviews, in press
Jordan, C. & Montesinos, B. 1991, MNRAS 252, 21
Mason, H.E., Doschek, G.A., Feldman, U., & Bhatia, A.K. 1979, A&A 73, 74
Mewe, R., Raassen, A.J.J., Drake, J.J., et al. 2001, A&A 368, 888
Ness, J.-U., Mewe, R., Schmitt, J.H.M.M., & Raassen, A.J.J. 2002, in ASP Conf. Ser. 277: Stellar Coronae in the Chandra and XMM-NEWTON Era, 545
Ness, J.-U., Schmitt, J.H.M.M., Burwitz, V., et al. 2002, A&A 387, 1032
Ness, J.-U. & Wichmann, R. 2002b, Astronomische Nachrichten 323, 129
Ness, J.-U., Brickhouse, N.S., Drake, J.J., & Huenemoerder, D.P. 2003a, ApJ 598, 1277
Ness, J.-U., Schmitt, J.H.M.M., Audard, M., et al. 2003b, A&A 407, 347
Ness, J.-U., Güdel, M., Schmitt, J.H.M.M., et al. 2004, A&A in press
Ottmann, R. & Schmitt, J.H.M.M. 1996, A&A 307, 813
Pallavicini, R., Golub, L., Rosner, R., et al. 1981, ApJ 248, 279
Porquet, D., Mewe, R., Dubau, J., el al. 2001, A&A 376, 1113
Rosner, R., Tucker, W., & Vaiana, G.S. 1978, ApJ 220, 643
Sanz-Forcada, J., Maggio, A., & Micela, G. 2003, A&A 408, 1087
Schmitt, J.H.M.M. & Kürster, M. 1993, Science 262, 215
Schmitt, J.H.M.M., Haisch, B.M., & Drake, J.J. 1994, Science 265, 1420
Schmitt, J.H.M.M. 1996, IAU Symp. 176, 85
Schmitt, J.H.M.M., Drake, J.J., Stern, R.A., & Haisch, B.M. 1996, ApJ 457, 882
Schmitt, J.H.M.M. 1997, A&A 318, 215
Schmitt, J.H.M.M. & Favata, F. 1999, Nature 401, 44
Schmitt, J.H.M.M., Ness, J.-U., & Franco, G. 2004, A&A 412, 849
Testa, P., Drake, J.J., & Peres, G. 2004, ApJ in press

White, N.E., Culhane, J.L., Parmar, A.N., et al. 1986, ApJ 301, 262